JOURNAL OF THE AMERICAN CHEMICAL SOCIETY

Subscriber access provided by ISTANBUL TEKNIK UNIV

Article

Kinetics and Mechanism for the Reaction of Hexafluoroacetylacetone with CuO in Supercritical Carbon Dioxide

Michael Durando, Rachel Morrish, and Anthony J. Muscat

J. Am. Chem. Soc., **2008**, 130 (49), 16659-16668 • DOI: 10.1021/ja8050662 • Publication Date (Web): 17 November 2008

Downloaded from http://pubs.acs.org on February 8, 2009

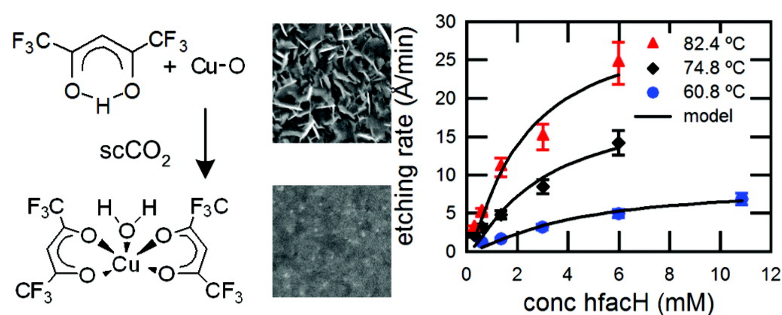

More About This Article

Additional resources and features associated with this article are available within the HTML version:

- Supporting Information
- Access to high resolution figures
- Links to articles and content related to this article
- Copyright permission to reproduce figures and/or text from this article

View the Full Text HTML

ACS Publications
High quality. High impact.

Journal of the American Chemical Society is published by the American Chemical Society. 1155 Sixteenth Street N.W., Washington, DC 20036

J|A|C|S
ARTICLES
Published on Web 11/17/2008

Kinetics and Mechanism for the Reaction of Hexafluoroacetylacetone with CuO in Supercritical Carbon Dioxide

Michael Durando, Rachel Morrish, and Anthony J. Muscat*

Department of Chemical and Environmental Engineering, University of Arizona, Tucson, Arizona 85721

Received July 1, 2008; E-mail: muscat@erc.arizona.edu

Abstract: A kinetic model and mechanism were developed for the heterogeneous chelation reaction of thin CuO films with hexafluoroacetylacetone (hfacH) in supercritical CO_2. This reaction has relevance for processing nanoscale structures and, more importantly, serves as a model system to tune the reaction behavior of solids using supercritical fluids. Precise control over reaction conditions enabled accurate etching rates to be measured as a function of both temperature [(53.5−88.4) ± 0.5 °C] and hfacH concentration (0.3−10.9 mM), yielding an apparent activation energy of 70.2 ± 4.1 kJ/mol and an order of approximately 0.6 with respect to hfacH. X-ray photoelectron spectroscopy and scanning electron microscopy were used to characterize the CuO surface, and a maximum etching rate of 24.5 ± 3.1 Å/min was obtained. Solvation forces between hfacH and the dense CO_2 permitted material removal at temperatures more than 100 °C lower than that of the analogous gas-phase process. In the low concentration regime, the etching reaction was modeled with a three-step Langmuir−Hinshelwood mechanism. Small amounts of excess water nearly doubled the reaction rate through the proposed formation of a hydrogen-bonded hfacH complex in solution. Further increases in the hfacH concentration up to 27.5 mM caused a shift to first-order kinetics and an adsorption-limited or Rideal−Eley mechanism. These results demonstrate that relatively modest increases in concentration can prompt a heterogeneous reaction in supercritical CO_2 to switch from a mechanism most commonly associated with a low-flux gas to one emblematic of a high-flux liquid.

Introduction

Fabrication of reduced-dimension metal structures with thermal, electronic, optical, and magnetic properties distinct from those of their bulk counterparts depends on control of reactions at solid surfaces. Currently, deposition and etching processes are used to manufacture metal wires, gratings, and contacts uniformly over a wide area, but new techniques that allow atomic level control over metal growth and removal could enable advanced architectures. Chelation reactions, where an organic ligand reversibly binds to a metal species, are emerging as a reliable method to deposit and etch metal layers. While chelators have long been used to stabilize and extract contaminants from water,[1] fuel,[2] and even the human body,[3] their interactions with solid surfaces is still a new area of research. The charge density and size of a chelator molecule, as well as the number and type of functional groups and their response to reaction conditions, all impact surface reactions with metal atoms. During deposition, a metal−chelate complex is chemically reduced to yield a surface-bound metal species and volatile organic ligands. The process can be reversed by reacting metal with a chelator at lower temperatures for material removal. Organometallic chelating reactions offer distinct advantages for nanoscale metal processing, such as uniform deposition and removal, specificity toward metal species, and compatibility with a variety of metal types.

Much of the research on heterogeneous metal chelation chemistry has focused on reactions in the gas phase, but recently we and others have reported that metals can be etched using β-diketone chelators dissolved in supercritical carbon dioxide ($scCO_2$).[4−10] Interest in $scCO_2$ technology has surged over the past 10 years due in large part to increasing environmental awareness for alternative solvents. In contrast with most organic solvents that have to be treated and disposed of as hazardous waste, carbon dioxide is nontoxic and nonflammable and can be cleanly separated and removed from a system by depressurization. There are also technical advantages gained by using $scCO_2$. The unique physicochemical properties of supercritical fluids have been extensively reviewed[11−13] and are evidenced by their incorporation into the pharmaceutical,[14,15] plastics,[16,17]

(1) Murphy, J. M.; Erkey, C. *Environ. Sci. Technol.* **1997**, *31*, 1674.
(2) Sievers, R. E.; Sadlowski, J. E. *Science* **1978**, *201*, 217.
(3) Richardson, D. R.; Tran, E. H.; Ponka, P. *Blood* **1995**, *86*, 4295.
(4) Murzin, A. A.; Babain, V. A.; Shadrin, A. Y.; Kamachev, V. A.; Strelkov, S. A.; Kiseleva, R. N.; Shafikov, D. N.; Podoinitsyn, S. V.; Kovalev, D. N. *Radiochemistry (Moscow)* **2003**, *45*, 131.
(5) Bessel, C. A.; Denison, G. M.; DeSimone, J. M.; DeYoung, J.; Gross, S.; Schauer, C. K.; Visintin, P. M. *J. Am. Chem. Soc.* **2003**, *125*, 4980.
(6) Xie, B.; Finstad, C. C.; Muscat, A. J. *Chem. Mater.* **2005**, *17*, 1753.
(7) Wang, J. S.; Wai, C. M. *Ind. Eng. Chem. Res.* **2005**, *44*, 922.
(8) Visintin, P. M.; Bessel, C. A.; White, P. S.; Schauer, C. K.; Desimone, J. M. *Inorg. Chem.* **2005**, *44*, 316.
(9) Shan, X.; Watkins, J. J. *Thin Solid Films* **2006**, *496*, 412.
(10) Skaf, D. W.; Kandula, S.; Harmonay, L.; Shodder, P.; Bessel, C. A.; Weinstein, R. D. *Ind. Eng. Chem. Res.* **2006**, *45*, 8874.

10.1021/ja8050662 CCC: $40.75 © 2008 American Chemical Society

environmental remediation,[18,19] and food manufacturing industries.[20] As a platform for chemical reactions, $scCO_2$ provides a tunable liquidlike density capable of solvating high concentrations of reagents combined with gaslike viscosity and diffusivity for enhanced reaction rates at relatively low temperatures. When working with nanoscale materials, the negligible surface tension of $scCO_2$ offers the additional benefit of rapid, nondestructive wetting regardless of feature size.

This study looked specifically at the surface reaction between CuO thin films and the β-diketone chelator, hexafluoroacetylacetone (hfacH), in an $scCO_2$ solvent. The high reactivity and widespread use of hfacH make it an ideal reactant for studying heterogeneous chelation mechanisms in $scCO_2$. When copper is in an oxidized state, it can undergo nucleophilic attack by hfacH, producing water and a volatile metal chelate, $Cu(hfac)_2$ (eq 1).[9,21,22] The metal chelate is highly hygroscopic and often combines with the product water, forming the bis monohydrate product $Cu(hfac)_2 \cdot H_2O$.[23] Other metals including Zn,[8,24,25] Pb,[24] and Ni[26] can be etched with a similar reaction scheme. The overall gas-phase reaction of CuO with hfacH is exothermic ($\Delta H_{rxn}° = -41.5$ kJ/mol)[27,28] and, by supplying additional heat, can be reversed to deposit copper oxide films.[29] Reaction of Cu(II) with hfacH has previously been used to extract copper ions from aqueous solutions[1,30] in addition to removing oxidized copper films in the gas[21,24,31,32] and supercritical[6] phases. While pure Cu metal cannot be directly etched by reaction with β-diketones, the chelation process can be combined with a simultaneous oxidation step to convert copper to either a +1 or +2 oxidation state, rendering it susceptible to attack.[5,8,10,22,33−35]

$$CuO + 2hfacH \leftrightarrow Cu(hfac)_2 + H_2O \leftrightarrow Cu(hfac)_2 \cdot H_2O \qquad (1)$$

Activation energies for the gas-phase reaction of β-diketones with Cu metal using O_2 as an in situ oxidant vary depending on the specific temperatures examined, but are reported in the range from approximately 30 to 50 kJ/mol.[33−35] Direct reaction of CuO with gas-phase hfacH yielded an apparent activation energy of 101.3 kJ/mol between 210 and 300 °C[32] but, when examined by thermogravimetric analysis in a different study, revealed a range of activation energies between 44 and 81 kJ/mol depending on the reaction step.[31] Energetic barriers for copper etching in $scCO_2$ have also been studied. The $scCO_2$ reaction of Cu_2O with an organic oxidizing agent, *tert*-butyl peracetate (*t*-BuPA), and 1,1,1-trifluoroacetylacetone (tfacH), where one CF_3 moiety in hfacH is replaced by a methyl group, showed an activation energy of 53 kJ/mol.[10] The activation energy of Cu_2O reacting with another β-diketone, 2,2,7-trimethyl-3,5-octanedione, in $scCO_2$ was 66 kJ/mol.[9] Few studies have been performed investigating the reaction orders for copper etching with hfacH. For gas-phase etching of Cu metal with O_2 and hfacH, the reaction exhibited a stoichiometric hfacH reaction order of 2 using high hfacH/O_2 ratios, but dropped to an order of 0.25 under highly oxidizing conditions.[34] Reacting Cu metal with *t*-BuPA and tfacH in $scCO_2$ was second-order with respect to tfacH and independent of the *t*-BuPA concentration.[10] When Cu_2O was etched under the same conditions, the reaction decreased to first-order in both tfacH and *t*-BuPA.[10]

Detailed studies of reaction mechanisms for metal chelation in $scCO_2$ are needed to extend the utility of this fluid. Quantifying kinetics and isolating the rate-determining step will improve control of the etching reaction and facilitate design and optimization of new methods for materials processing. Moreover, developing a mechanistic model of the chelation process will contribute to the fundamental understanding of heterogeneous reactions in supercritical fluids and provide insight into the types of reactive pathways that are best suited for $scCO_2$. The temperature- and pressure-sensitive kinematic properties that make $scCO_2$ such a versatile solvent also present challenges when trying to quantify reaction rates. Exacting control of reaction conditions is required to ensure that inadvertent fluctuations in solvent properties do not compromise the measured rate. In this study, the kinetics of etching CuO with hfacH in $scCO_2$ were measured using X-ray photoelectron spectroscopy (XPS) and scanning electron microscopy (SEM) to characterize the metal surface. Precise measurements of the etching rate were obtained through stringent control of $scCO_2$ processing conditions over a temperature range of 53.5− 88.4 °C and an hfacH concentration of 0.3−27.5 mM. The effects of adding the reaction products $Cu(hfac)_2 \cdot H_2O$ and H_2O were examined, and a mechanism is proposed that is consistent with the experimental results for the heterogeneous reaction.

Experimental Methods

CuO Sample Preparation. Uniform CuO layers were formed by ex situ oxidization of copper metal films. Si(100) wafers (4 in., p-type, 0.001−0.02 Ω cm) were cleaned in piranha solution (5:1 by volume H_2SO_4/H_2O_2) followed by dipping in 0.5 vol % HF for 10 min to obtain a hydrogen-terminated surface. A 200 Å Cr adhesion layer was deposited by electron beam evaporation (Edwards, Auto 306) directly onto the wafer surface followed by a 2000 Å copper metal layer. X-ray diffraction with unfiltered Kα radiation (Philips X'pert MPD) confirmed a typical ⟨111⟩ crystal structure of the prepared Cu films. The copper metal was oxidized by a 6 min exposure in 10% by volume aqueous H_2O_2 (class 10, General Chemical) in 18 MΩ cm ultrapure water at 25 °C. This

(11) Savage, P. E.; Gopalan, S.; Mizan, T. I.; Martino, C. J.; Brock, E. E. *AIChE J.* **1995**, *41*, 1723.
(12) Eckert, C. A.; Knutson, B. L.; Debenedetti, P. G. *Nature* **1996**, *383*, 313.
(13) Beckman, E. J. *J. Supercrit. Fluids* **2004**, *28*, 121.
(14) Palakodaty, S.; York, P. *Pharm. Res.* **1999**, *16*, 976.
(15) Subramaniam, B.; Rajewski, R. A.; Snavely, K. *J. Pharm. Sci.* **1997**, *86*, 885.
(16) Canelas, D. A.; Burke, A. L. C.; DeSimone, J. M. *Plast. Eng. (Brookfield, Conn.)* **1997**, *53*, 37.
(17) Kendall, J. L.; Canelas, D. A.; Young, J. L.; DeSimone, J. M. *Chem. Rev.* **1999**, *99*, 543.
(18) Brady, B.; Kao, C. P. C.; Dooley, K. M.; Knopf, F. C.; Gambrell, R. P. *Ind. Eng. Chem. Res.* **1987**, *26*, 261.
(19) Bowadt, S.; Hawthorne, S. B *J. Chromatogr., A* **1995**, *703*, 549.
(20) Palmer, M. V.; Ting, S. S. T. *Food Chem.* **1995**, *52*, 345.
(21) George, M. A.; Hess, D. W.; Beck, S. E.; Ivankovits, J. C.; Bohling, D. A.; Lane, A. P. *J. Electrochem. Soc.* **1995**, *142*, 961.
(22) Jain, A.; Kodas, T. T.; Hampden-Smith, M. J. *Thin Solid Films* **1995**, *269*, 51.
(23) Kodas, T.; Hampden-Smith, M. *The Chemistry of Metal CVD*; VCH: Weinheim, Germany, 1994.
(24) Rousseau, F.; Jain, A.; Kodas, T. T.; Hampden-Smith, M.; Farr, J. D.; Meunchausen, R. *J. Mater. Chem.* **1992**, *2*, 893.
(25) Droes, S. R.; Kodas, T. T.; Hampden-Smith, M. J. *Adv. Mater.* **1998**, *10*, 1129.
(26) Nigg, H. L.; Masel, R. I. *J. Vac. Sci. Technol., A* **1999**, *17*, 3477.
(27) da Silva, M. A. V. R.; Ferrao, M. L. C. C. H. *J. Chem. Thermodyn.* **1988**, *20*, 359.
(28) da Silva, M. A. V. R.; Goncalves, J. M.; Pilcher, G. *J. Chem. Thermodyn.* **1997**, *29*, 253.
(29) Pinkas, J.; Huffman, J. C.; Baxter, D. V.; Chisholm, M. H.; Caulton, K. G. *Chem. Mater.* **1995**, *7*, 1589.
(30) Smart, N. G.; Carleson, T.; Kast, T.; Clifford, A. A.; Burford, M. D.; Wai, C. M. *Talanta* **1997**, *44*, 137.
(31) Sekiguchi, A.; Kobayashi, A.; Koide, T.; Okada, O.; Hosokawa, N. *Jpn. J. Appl. Phys.* **2000**, *39*, 6478.
(32) Lee, W.; Yang, H.; Reucroft, P. J.; Soh, H.; Kim, J.; Woo, S.; Lee, J. *Thin Solid Films* **2001**, *392*, 122.
(33) Kruck, T.; Schober, M. *Microelectron. Eng.* **1997**, *37/38*, 121.
(34) Steger, R.; Masel, R. *Thin Solid Films* **1999**, *342*, 221.
(35) Kang, S.; Kim, H.; Rhee, S. *J. Vac. Sci. Technol., B* **1999**, *17*, 154.

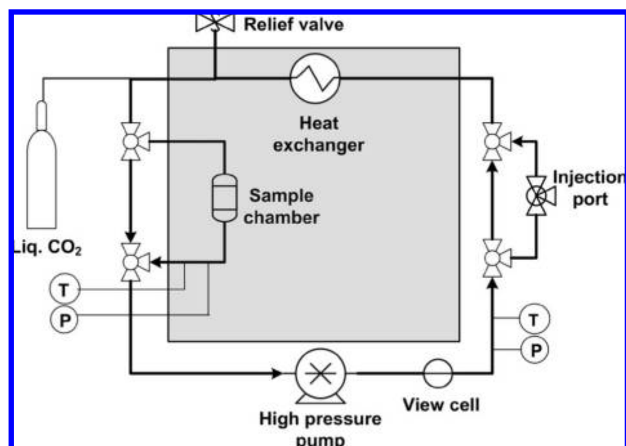

Figure 1. Schematic of the high-pressure recirculating batch reactor. The shaded area represents portions of the reactor enclosed in an oven.

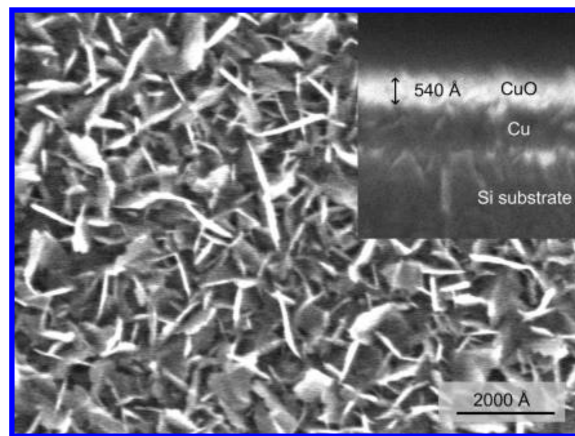

Figure 2. Top-down and cross-sectional (inset) FESEM images of the samples used for CuO etching studies.

self-limiting oxidation method has been shown to reproducibly form ~500 Å CuO films.[36] Samples of approximately 1.25 cm^2 were cut from a wafer and used for experimentation.

Reactor System. A schematic of the high-pressure, recirculating batch reactor system designed for kinetic investigations in $scCO_2$ is shown in Figure 1. The 250 mL stainless steel reactor contained a heat exchanger coil, a 4 mL removable sample chamber, a 2 mL chemical injection port, and a view cell for visualization of the CO_2 state. Approximately 90% of the reactor system including the sample chamber was located within a standard laboratory oven (Blue M 1000). Portions outside the oven were heated resistively. Pressurized CO_2 was circulated via a high-pressure, positive-displacement pump (Micropump Inc. 415a). The system was automated by a custom program written in Labview (National Instruments). This program controlled multiple air-actuated valves and acquired incremental temperature (Omega KQXL) and pressure (Omega PX4100) values in both the sample chamber and circulation loop. The set point accuracy was ±0.5 °C and ±1 bar. Temperature was regulated with on/off control of the oven (Omega CNi3244), and pressure was set by venting small amounts of CO_2. A pressure relief valve was included for safety. The entire system was tested to 150 °C and 300 bar; typical operating conditions were 50−90 °C and 185 bar.

Sample Processing and Characterization. To ensure precise rate measurements, the reactor was configured to process samples in a well-mixed $scCO_2$ solution under conditions that remained constant during an entire experiment. A full description of the reactor flow paths and sample exposure methods is given in the Supporting Information. Briefly, CuO samples were etched with hfacH (Alfa Aesar, 99.9%) dissolved in $scCO_2$ (99.99%) at temperatures ranging from 53.5 to 88.4 °C and a constant pressure of 185 bar. This pressure gave a dense CO_2 solution capable of solvating all reactive species over the range of temperatures examined. hfacH concentrations of 0.3−27.5 mM were chosen to maintain a negligible change in reactant concentration during an experiment while concurrently generating a reaction rate that was slow enough to be accurately measured. Kinetic effects of the etching products were investigated by adding both ultrapure H_2O (18 MΩ cm) at concentrations of 0−12.4 mM and $Cu(hfac)_2 \cdot H_2O$ (Alfa Aesar) at concentrations of 0−9.0 mM as coreagents to the $scCO_2$ mixture. Using automatically controlled flow loops, the reactants were first mixed into the heated CO_2, and then the homogeneous etching solution was exposed to the sample chamber for a set reaction time (18−420 min). After processing, the samples were rinsed with both liquid CO_2 and purified hexanes (Aldrich, 99%) and then rapidly transferred to an ultra-high-vacuum chamber (10^{-9} Torr) for characterization. Total sample exposure to the clean room atmosphere was less than 5 min.

Surface species were analyzed using an X-ray photoelectron spectrometer (Physical Electronics, model 549) with a double-pass cylindrical mirror analyzer and a 400 W X-ray gun (Al Kα radiation). Approximately 45 high-resolution scans at a pass energy of 25 eV in the Cu 2p binding energy range from 970 to 930 eV were coadded to determine the oxidation state of the copper surface. Full survey spectra were taken at a 200 eV pass energy. All XPS spectra were aligned on the basis of adventitious C 1s at 284.6 eV. Spectra were fit with a least-squares method using a Shirley background and Voigt line shapes for the purpose of deconvoluting into individual states and obtaining peak areas. The surface morphology of the copper layer was characterized with field emission (FE) SEM (Hitachi S-4500). The samples did not require a conductive coating, and both top-down and cross-sectional images were taken.

The nominal etching rate was calculated by determining the amount of time necessary to completely remove the CuO layer. After etching, each sample was analyzed by XPS to detect the presence of CuO. Observation of CuO indicated the reaction time was insufficient to completely remove the film. Subsequent samples were exposed to hfacH under identical conditions but for longer periods of time until no CuO was visible in the Cu 2p region. Conversely, if the initial experiment at a set of operating conditions indicated complete removal of the CuO film, the next experiments would repeat exposure at shorter times until CuO was visible in the postetch XPS analysis. Iterations were performed to bracket the etching time by a 10% relative error defined when the CuO $2p_{3/2}$ XPS peak passes the threshold limit of detection; the nominal etching rate was determined by dividing the CuO film thickness by the removal times and averaging the results. Repeat experiments of the etching rate were consistent and showed that variations in the operating conditions of less than ±0.5 °C and ±1 bar were negligible.

Results

Sample characterization. Figure 2 shows top-down and cross-sectional (inset) SEM images of a prepared CuO surface after oxidation. CuO films grown in this manner have a characteristic rough, shardlike morphology caused by the formation of lower density CuO from a smooth Cu metal film.[22] Digital SEM image analysis using a Sobel algorithm for edge delineation was used to estimate an average CuO thickness of 540 Å and a standard deviation of 80 Å over a 1 μm wide cross-sectional region. Although microscope resolution and slight variations in the normal planarity of a sample could impact SEM thickness measurements, the calculated average height of 540 Å is

(36) Nishizawa, H.; Tateyama, Y.; Saitoh, T. *Thin Solid Films* **2004**, *455*, 491.

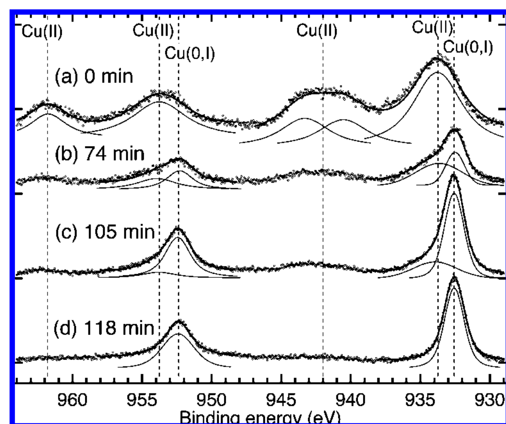

Figure 3. XPS spectra in the 2p energy range for CuO films exposed to 1.4 mM hfacH in $scCO_2$ at 74.8 °C and 185 bar for (a) 0, (b) 74, (c) 105, and (d) 118 min.

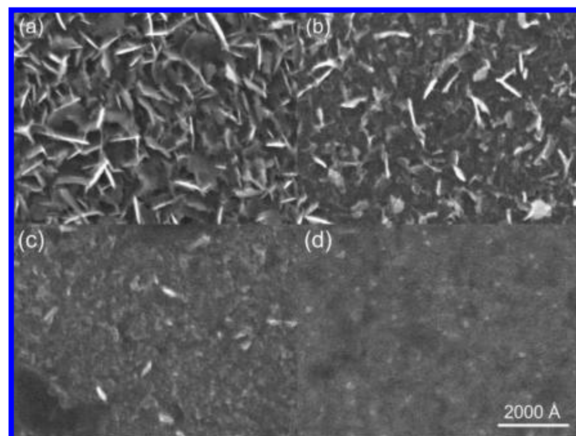

Figure 4. Top-view FESEM images of CuO films processed with 1.4 mM hfacH at 74.8 °C and 185 bar for increasing times: (a) 0, (b) 74, (c) 90, and (d) 118 min. The scale bar applies to all four images.

substantiated by a reported self-limiting CuO oxidation threshold of ~500 Å.[36] The computed 80 Å standard deviation provides an estimate of the variation in the CuO film thickness. Using conventional error propagation techniques, the variability of the CuO film height can be averaged with the 10% uncertainty in CuO removal time to determine an overall error in the measured rate. The coarse CuO morphology combined with the relative thinness of the film presented challenges in accurately characterizing the receding oxide layer with common analysis tools including ellipsometry and profilometery. XPS was chosen because it is a nondestructive technique that provided both the sensitivity and precision necessary to determine angstrom per minute etching rates.

An example series of high-resolution XPS spectra showing the gradual removal of CuO with time in the hfacH etchant solution is given in Figure 3. The progression is representative of the stepwise etching experiments performed in this study. Each spectrum is from a separate CuO sample etched with 1.4 mM hfacH in $scCO_2$ at 74.8 °C and 185 bar. Prior to etching, the spectra contained a copper $2p_{1/2}$ peak at 953.7 eV and a $2p_{3/2}$ peak at 933.7 eV (Figure 3a). These binding energies are 1.3 ± 0.2 eV higher than the peak positions for Cu(0) metal and were assigned to oxidized Cu(II).[37,38] The broadness and slight asymmetry of the CuO 2p peaks result from multiplet splitting.[37] Strong shakeup satellite peaks present at ~962 eV and an overlapping series at ~942 eV confirm the Cu(II) surface. $Cu(OH)_2$ XPS spectra also contain satellite peaks, but this species was ruled out because the 2p binding energy shift is higher (2.5 ± 0.15 eV) relative to that of Cu(0).[37] The intensity of the Cu(II) shakeup satellite peaks decreased with longer exposure times in the etching solution (Figure 3b,c). After a reaction time of 118 min, there were no distinguishable satellite lines and the spin−orbit-coupled Cu 2p region was fit with a set of single peaks at lower binding energies of 952.4 ($2p_{1/2}$) and 932.6 eV ($2p_{3/2}$) (Figure 3d). These positions are consistent with either Cu(0) or Cu(I), indicating the Cu(II) layer had been fully etched.[38] The removal time of the 540 Å CuO film under these conditions was bracketed between 105 and 118 min, yielding a nominal etching rate of 4.8 ± 0.5 Å/min. The escape depth of photoelectrons limits monitoring variations in the etching rate with film thickness to the last ~50 Å before the film was cleared. Although CuO XPS peak areas obtained in this thickness range varied linearly with time, only nominal etching rates are reported.

Corresponding top-view SEM images for samples exposed to 1.4 mM hfacH in $scCO_2$ solution at 74.8 °C and 185 bar for increasing reaction times are shown in Figure 4. Prior to etching, the surface exhibited a coarse morphology indicative of CuO. As etching progressed, the roughness of the CuO features was reduced, which matches the decreasing oxide intensity seen in the high-resolution XPS spectra (Figure 3). Once all of the oxide was removed, a nearly smooth copper surface was observed (Figure 4d). Note that the SEM image in Figure 4c has a shorter reaction time (90 min) than the corresponding XPS spectrum in Figure 3c (105 min) because the surface morphology was indistinguishable between the 105 and 118 min samples.

XPS survey spectra of the starting CuO film over the binding energy range 1000−0 eV showed superficial Cu(II) and O, as well as adventitious C (see Figure S2, Supporting Information). After CuO removal was complete on the basis of high-resolution data, a low-intensity O peak was still observed in the survey scan; this O signal likely came from Cu_2O, which contains Cu(I), and has a 2p peak position identical to that of Cu(0) metal. Control experiments exposing a pure evaporated Cu(0) film to ambient conditions for 5 min produced an O peak with intensity comparable to that of the fully etched samples, indicating a thin layer of Cu_2O formed during the short exposure to the atmosphere between etching and analysis in the XPS chamber. Initial studies also showed residual F contamination from hfacH. The F was reduced by including a liquid CO_2 cleaning step along with a rinse in purified hexanes, which have solvation properties comparable to those of $scCO_2$. After $scCO_2$ etching, a "grass green" precipitate product collected in the reactor exhaust. This specific coloring matches the bis monohydrate product $Cu(hfac)_2 \cdot H_2O$, though lesser amounts of other products such as purple-colored anhydrous $Cu(hfac)_2$ cannot be discounted.[23]

Arrhenius Analysis. An Arrhenius plot of the etching rate over a 35 °C temperature interval can be fit with a single line as shown in Figure 5. The error bars represent the propagated error due to uncertainties in the etching time (±10%) and CuO layer thickness (±80 Å). The etching rate was measured at six temperatures in the interval from 53.5 to 88.4 °C (±0.5 °C) at a constant hfacH concentration of 3.0 mM and a pressure of

(37) McIntyre, N. S.; Sunder, S.; Shoesmith, D. W.; Stanchell, F. W. *J. Vac. Sci. Technol.* **1981**, *18*, 714.
(38) Moulder, J. F.; Stickle, W. F.; Sobol, P. E.; Bomben, K. D. *Handbook of X-ray Photoelectron Spectroscopy*; Physical Electronics, Inc.: Eden Prairie, MN, 1995.

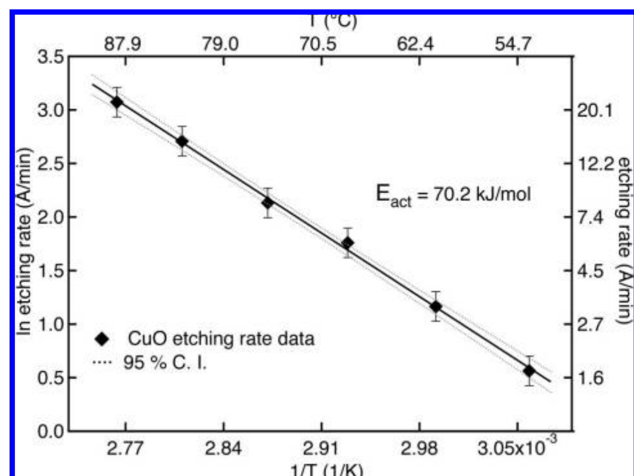

Figure 5. Temperature dependence of the CuO etching rate between 53.5 and 88.4 °C at 185 bar and 3.0 mM hfacH. The error bars correspond to the propagated error from uncertainties in the CuO film thickness and etching time. The solid line is a linear least-squares fit of the data, and the dotted lines show the 95% CI. The slope of the fit yields an activation energy of 70.2 ± 4.1 kJ/mol.

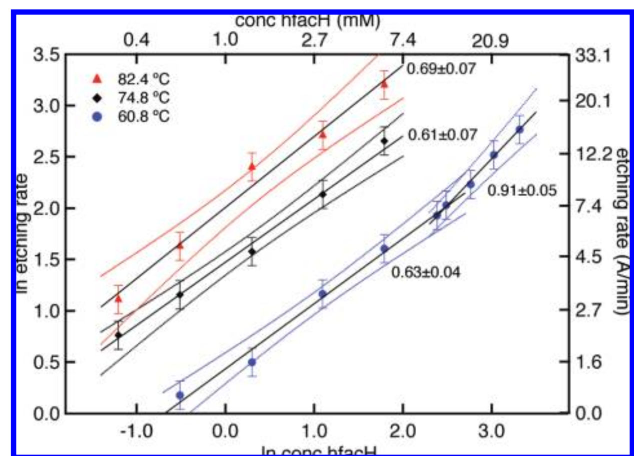

Figure 6. Dependence of the CuO etching rate on the hfacH concentration at 60.8, 74.8, and 82.4 °C. The error bars correspond to the propagated error from uncertainties in the CuO film thickness and etching time. The solid lines are linear least-squares fits of the data, and the dotted lines represent the corresponding 95% CI. The reaction orders shown are the slopes of the fits in each concentration interval, and the uncertainties are ±1 SD.

185 bar (±1 bar). Maintaining a constant pressure over this temperature range resulted in an approximately 0.25 g/mL variation in solvent density on the basis of the Peng−Robinson equation of state for pure CO_2. The apparent activation energy obtained from the slope of a linear fit is 70.2 ± 4.1 kJ/mol. Least-squares analysis of the data showed a correlation of greater than 0.99 and also provided a 95% CI for the linear fit shown in Figure 5.

hfacH Concentration Dependence. The effect of the hfacH concentration on the etching rate was studied at three different midrange processing temperatures of 60.8, 74.8, and 82.4 °C (Figure 6). All experiments were carried out at 185 bar. Dilute hfacH concentrations of less than 30 mM were used to minimize nonsurface reaction related factors, including mass transport limitations and solution-phase reactant−reactant interactions. The reduced reaction rate at 60.8 °C permitted the etching reaction to be measured over nearly 2 orders of magnitude variation in the hfacH concentration, from 0.6 to 27.5 mM. The

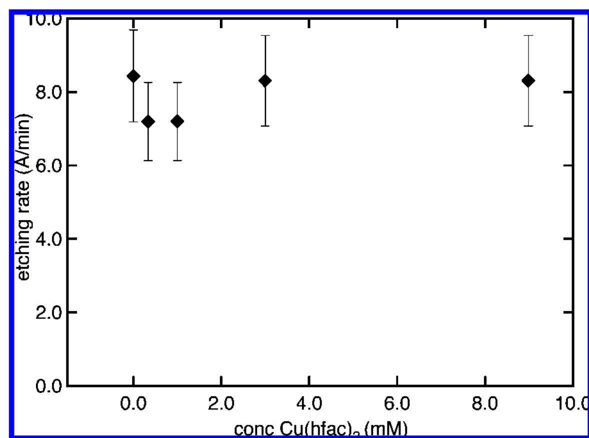

Figure 7. Dependence of the CuO etching rate on the $Cu(hfac)_2 \cdot H_2O$ concentration at 74.8 °C and 185 bar with a constant hfacH concentration of 3.0 mM. The error bars correspond to the propagated error from uncertainties in the CuO film thickness and etching time.

two higher temperatures of 74.8 and 82.4 °C were studied over a lower range of 0.3−6.0 mM hfacH because etching rates above ∼25 Å/min could not be accurately measured. Least-squares analysis showed apparent reaction orders of 0.61 ± 0.07 and 0.69 ± 0.07 at processing temperatures of 74.8 and 82.4 °C, respectively. The rate data gathered at 60.8 °C exhibited two distinguishable regions. Below 11 mM, an apparent order of 0.63 ± 0.04 was observed, while at higher hfacH concentrations, the order increased to 0.91 ± 0.05. The uncertainty in reaction orders was determined from the linear fit of the etching data. At the conditions employed in this study, the highest etching rate measured was 24.5 ± 3.1 Å/min (∼9 CuO layers/min) at 82.4 °C with 6.0 mM hfacH.

Effect of $Cu(hfac)_2 \cdot H_2O$ and H_2O. Potential product inhibition mechanisms were explored by measuring CuO etching rates in the presence of the reaction products $Cu(hfac)_2 \cdot H_2O$ and pure water (eq 1). The effect of adding the etching product $Cu(hfac)_2 \cdot H_2O$ as a reagent was studied at a midrange temperature of 74.8 °C, 185 bar, and a constant hfacH concentration of 3.0 mM. $Cu(hfac)_2 \cdot H_2O$ was added at concentrations of 0.33−9.0 mM, which are below the reported solubility limit in $scCO_2$.[39] Figure 7 shows the measured etching rate as a function of the $Cu(hfac)_2 \cdot H_2O$ concentration. Observation of a nearly constant reaction rate indicates that the etching process exhibited zeroth-order dependence on $Cu(hfac)_2 \cdot H_2O$ even at high concentrations of 9.0 mM, which is over 3000 times the concentration produced by etching the entire 540 Å CuO layer.

Addition of pure water as a coreagent had a markedly different effect, causing a significant enhancement of the reaction rate. Figure 8 shows the increasing etching rate as a function of the H_2O concentration studied at 74.8 °C, 185 bar, and a constant hfacH concentration of 1.4 mM. A lower hfacH concentration was required when water was added to maintain a slow, measurable etching rate. The variation of the water concentration corresponds to 3−20 times the stoichiometric ratio of H_2O to hfacH on the basis of eq 1, but is below reported solubility limits of water in pure $scCO_2$.[40] At approximately 10× molar excess (6.2 mM), the catalytic effect of water saturated and no additional increase in rate was observed. The increase in rate attributed to water was approximated by

(39) Lagalante, A. F.; Hansen, B. N.; Bruno, T. J. *Inorg. Chem.* **1995**, *34*, 5781.
(40) Wiebe, R.; Gaddy, V. L. *J. Am. Chem. Soc.* **1941**, *63*, 475.

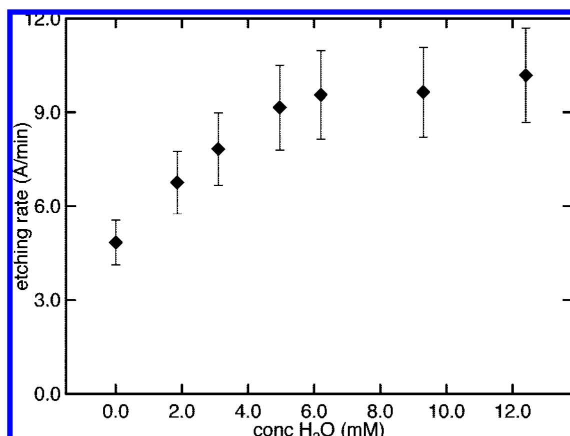

Figure 8. Dependence of the CuO etching rate on the H_2O concentration at 74.8 °C and 185 bar with a constant hfacH concentration of 1.4 mM. The error bars correspond to the propagated error from uncertainties in the CuO film thickness and etching time.

subtracting the pure hfacH etching rate ($C_{H_2O} = 0$ mM) from the total measured reaction rate and showed a reaction order of 0.77 ± 0.06 below 10× H_2O concentration. Control experiments evaluating the sole effect of water on the sample surface were performed under identical etching conditions but using only 10× H_2O as a reactant. Neither a Cu metal nor a CuO surface showed changes in the Cu 2p XPS spectra after an extended 90 min exposure to pure water in $scCO_2$.

Scheme 1. Reaction Mechanism of CuO with hfacH in $scCO_2$[a]

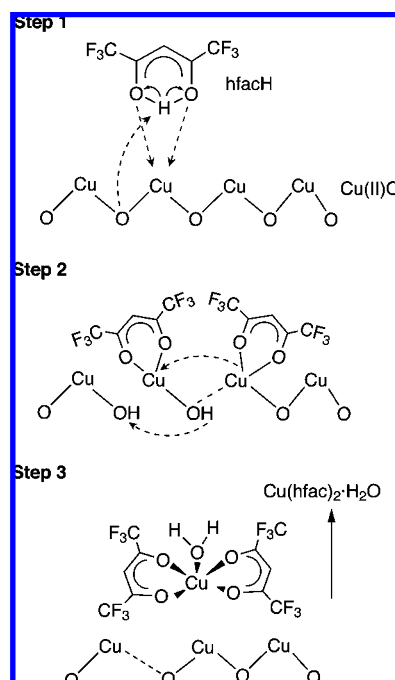

[a] Step 1 is adsorption of hfac ligand, forming ∼O−Cu−hfac and hydroxyl termination. Step 2 is Langmuir−Hinshelwood surface reaction to form surface-bound $Cu(hfac)_2$ and H_2O. Step 3 is desorption of $scCO_2$-soluble bis monohydrate product.

Discussion

Etching Mechanism. The overall reaction between hfacH and CuO forming soluble $Cu(hfac)_2$ and H_2O has been well documented in the literature and proceeds via eq 1.[6,9,31] XPS and SEM analysis confirmed etching of CuO films in hfacH/$scCO_2$ solution, producing a grass green precipitate predominantly composed of $Cu(hfac)_2 \cdot H_2O$. Over the temperature range studied, the heterogeneous reaction showed a nonelementary hfacH reaction order of approximately 0.6 at low concentrations and an increased order at higher concentrations. Adding the reaction products of $Cu(hfac)_2 \cdot H_2O$ and pure H_2O as reagents was expected to shift the reaction equilibrium toward the reactants, decreasing the etching rate. However, excess $Cu(hfac)_2 \cdot H_2O$ showed no measurable effect, and H_2O enhanced the rate. A reaction order of less than 1 combined with complex behavior of the reactive species suggests that etching occurs by a series of steps, one or more of which could be rate controlling.

Several mechanisms for heterogeneous Cu etching with hfacH have been proposed in the literature. One study suggests that the gas-phase reaction of hfacH with porous CuO wires between 170 and 240 °C occurs in a multistep process beginning with coordination of hfacH to Cu, forming an intermediate adsorbed Cu−hfac species ($E_A = 44$ kJ/mol).[31] Two neighboring Cu−hfac species react disproportionately to generate volatile $Cu(hfac)_2$ ($E_A = 81$ kJ/mol). A similar mechanism has been reported in the high-temperature (∼300 °C) gas-phase reaction of $Pd(hfac)_2$ with Cu metal to form Pd metal and $Cu(hfac)_2$.[41,42] The $Pd(hfac)_2$ species decomposes on a Cu surface into a Pd atom and hfac ligands. Diffusion of the ligands to a Cu site and subsequent reaction produces the metal chelate. In recent Cu etching work by our group, a model for Cu(II) island removal with hfacH in $scCO_2$ at 40−60 °C and 100−250 atm was presented.[6] Etching of Cu(II) was proposed to occur by sequential nucleophilic attack of two fluid-phase hfacH molecules on a CuO oligomer, with each hfacH separately cleaving a Cu−O bond, producing a terminal hydroxyl. Once flanked by two ligands, the copper dissolves into solution. Further reaction of hfacH with the hydroxylated ends of the oligomer chain produces water. The three published mechanisms agree that metal removal includes adsorption of hfacH and requires attachment of two hfac ligands to a surface-bound Cu atom, but differ in the surface reaction step. Additional mechanisms for etching Cu or copper oxides using hfacH and an oxidant have been published; however, they primarily focus on the reaction in the presence of a third reagent, adding another facet to the process.[8,10,22]

On the basis of kinetic and energetic results for the reaction of CuO thin films with hfacH in $scCO_2$ at 53.5−88.4 °C and 185 bar, we developed the stepwise mechanism shown in Scheme 1. In this mechanism, CuO is represented by an oligomer structure where each Cu atom is bound to two O atoms, forming a stoichiometric repeating unit. During Cu oxidation, O inserts into unoccupied tetrahedral sites, generating an interconnected CuO network with partial charges on each atom.[6] The CuO etchant hfacH is depicted in an enol conformation where a hydrogen atom sits between the two oxygen atoms, creating a central ring with delocalized bonding. β-Diketones typically undergo tautomeric equilibrium between keto and enol conformations, but the electron-withdrawing CF_3 groups on hfacH stabilize the enol form, making it the active species in nonpolar solvents such as $scCO_2$.[43]

The etching reaction is initiated by hfacH adsorbing dissociatively on the CuO surface, forming ∼O−Cu−hfac and

(41) Lin, W.; Wiegand, B. C.; Nuzzo, R. G.; Girolami, G. S. *J. Am. Chem. Soc.* **1996**, *118*, 5977.
(42) Lin, W.; Nuzzo, R. G.; Girolami, G. S. *J. Am. Chem. Soc.* **1996**, *118*, 5988.

Cu−OH, which is shown in step 1 of the reaction mechanism (Scheme 1). As a fluid-phase hfacH approaches the metal surface, the acidic hydrogen at the center of the enol conformer transfers to an electronegative O atom, creating a hydroxyl termination and weakening or breaking the Cu−O bond. The conjugated nucleophilic ring of the hfac anion bonds with the positively charged Cu atom to form ∼O−Cu−hfac. Ultra-high-vacuum studies of hfacH chemisorption on Cu surfaces have shown that hfacH readily chemisorbs above 150 K in the standing up conformation depicted in step 1.[44] Reaction of another hfacH molecule from the fluid with a hydroxylated Cu atom produces a water molecule and ∼O−Cu−hfac.

In step 2, a second hfacH molecule reacts by one of two mechanisms. The first is a Langmuir−Hinshelwood sequence where two adsorbed hfac moieties react, forming $Cu(hfac)_2$ and a vacant CuO site. Alternatively, the reaction could follow a Rideal−Eley sequence where an hfacH molecule from the fluid phase reacts directly with ∼O−Cu−hfac on the surface. Langmuir−Hinshelwood kinetics typically dominates in gas-phase reactions where the flux of reactants to the surface is low, but the relatively high reactant concentrations in supercritical fluids make Rideal−Eley kinetics equally plausible. Kinetic models were developed for both Langmuir−Hinshelwood and Rideal−Eley mechanisms, but only the former was able to accurately model a reaction order of less than 1. The primary difference is that the two reacting species are both adsorbed on surface sites in a Langmuir−Hinshelwood mechanism, whereas only one adsorbed species is required in a Rideal−Eley mechanism. A Langmuir−Hinshelwood sequence was used to model the kinetics of CuO etching in $scCO_2$ in the low hfacH concentration regime (<11 mM).

In step 2 of Scheme 1, a second hfacH molecule must either directly adsorb or diffuse on the surface to a site neighboring an existing ∼O−Cu−hfac species. This process is inherently slow because direct adsorption is sterically hindered by the bulky standing up conformation of the first adsorbed hfac and surface diffusion of ligands is limited by the low temperature used in $scCO_2$ processing. Once two adjacent CuO sites are occupied by adsorbed hfacH, the lower ΔH_f of the etching products drives transfer of a ligand from one Cu atom to another. Similarly, one of the two proximal hydroxyl groups releases a proton to the other. These reactions generate surface-bound $Cu(hfac)_2$ and water and form an open CuO site from the vacated Cu and O atoms.

The last step of CuO etching in $scCO_2$ is desorption of both the chelate product and water as illustrated in Scheme 1, step 3. Since $Cu(hfac)_2 \cdot H_2O$ was the primary product observed, we can conclude that either $Cu(hfac)_2$ and H_2O desorb separately and then combine in the fluid phase or the two adsorbed species react to form the hydrate on the surface and desorb together. Our studies did not permit distinction between the two processes, but if water and $Cu(hfac)_2$ do desorb separately, they likely combine close to the surface where the concentrations of product species are relatively high. The unstable dangling bonds on the Cu and O atoms left on either side of the removed CuO species could bond directly to each other or react immediately with another hfacH molecule. In the balanced reaction sequence, the former pathway was chosen and the reaction starts anew once the products desorb, exposing a fresh CuO site.

(43) Henry, M. C.; Yonker, C. M. *Anal. Chem.* **2004**, *76*, 4684.
(44) Girolami, G. S.; Jeffries, P. M.; Dubois, L. H. *J. Am. Chem. Soc.* **1993**, *115*, 1015.

Reaction Kinetics. Etching of CuO films in the low concentration regime occurs sequentially by dissociative adsorption of hfacH onto CuO (step 1), surface reaction between two adsorbed hfacH species (step 2), and finally desorption of the Cu chelate and water (step 3). Balanced equations for the three-step mechanism are given as eqs 2−4. Each CuO species is treated as a single surface site.

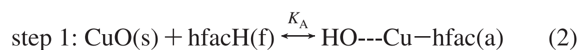

$$\text{step 1: CuO(s)} + \text{hfacH(f)} \xleftrightarrow{K_A} \text{HO---Cu−hfac(a)} \quad (2)$$

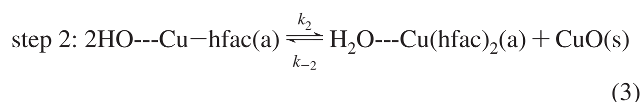

$$\text{step 2: 2HO---Cu−hfac(a)} \underset{k_{-2}}{\overset{k_2}{\rightleftharpoons}} \text{H}_2\text{O---Cu(hfac)}_2\text{(a)} + \text{CuO(s)} \quad (3)$$

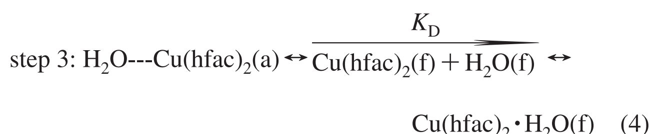

$$\text{step 3: H}_2\text{O---Cu(hfac)}_2\text{(a)} \leftrightarrow \xrightarrow{K_D} \text{Cu(hfac)}_2\text{(f)} + \text{H}_2\text{O(f)} \leftrightarrow \text{Cu(hfac)}_2 \cdot \text{H}_2\text{O(f)} \quad (4)$$

The zeroth-order dependence of the measured rate on $Cu(hfac)_2 \cdot H_2O$ indicates product desorption in step 3 proceeds rapidly and is not rate controlling (Figure 7). Since the initial chemisorption of hfacH on a Cu surface readily occurs at temperatures below those studied, it is more likely that step 2 is rate limiting. Additionally, choosing step 1 as rate controlling predicts an hfacH reaction order greater than 1 and results in a poor fit of the low-concentration experimental data. Step 2 was consequently chosen as rate limiting, and steps 1 and 3 were modeled under dynamic equilibrium. The overall reaction consumes one CuO species and two hfacH molecules and produces $Cu(hfac)_2 \cdot H_2O$ in solution. A site balance equating the sum of the fractional surface coverages for vacant CuO sites (θ_{CuO}), sites with one adsorbed ligand ($\theta_{HO-Cu-hfac}$), and sites with two adsorbed ligands ($\theta_{H_2O-Cu(hfac)_2}$) to unity

$$1 = \theta_{CuO} + \theta_{HO-Cu-hfac} + \theta_{H_2O-Cu(hfac)_2} \quad (5)$$

is combined with steps 1−3 to eliminate the surfaces coverages. This yields the following expression for the reaction rate:

$$r = \frac{K_D[k_2 K_A{}^2 K_D C_{hfacH}{}^2 - k_{-2} C_{Cu(hfac)_2 \cdot H_2O}]}{[C_{Cu(hfac)_2 \cdot H_2O} + (1 + K_A C_{hfacH}) K_D]^2} \quad (6)$$

where k_2 and k_{-2} are the forward and reverse reaction rate constants for step 2 and K_A and K_D are the equilibrium constants for adsorption (step 1) and desorption (step 3), respectively. The second-order dependence on the hfacH concentration in the numerator reflects the stoichiometry of the overall reaction, and its functionality in the denominator arises from hfac occupation of surface sites.

The proposed reaction model does not account for mass transfer resistance because etching of CuO with hfacH in $scCO_2$ was found to be surface reaction limited. A surface Damköhler number can be defined by

$$Da_s = \frac{rL}{x\mathscr{D}} \quad (7)$$

where r is the metal etching rate, L is the characteristic diffusion length to the metal surface, x is the fluid-phase reactant mole fraction, and $\mathscr{D}$ is the reactant diffusivity in solution.[23] Da_s for CuO etching in $scCO_2$ was approximated by choosing representative values of the etching rate (10 Å/min) and hfacH concentration (10^{-4} mole fraction) along with a conservative boundary layer thickness of 100 μm. The infinite dilution

Table 1. Fit of the Reaction Rate Parameters K_A and k_2 in a Langmuir–Hinshelwood Model at 60.8, 74.8, and 82.4 °C

temp (°C)	K_A (mM^{-1})	k_2 (Å/min)
60.8	0.51	9.2
74.8	0.75	20.2
82.4	0.98	31.5

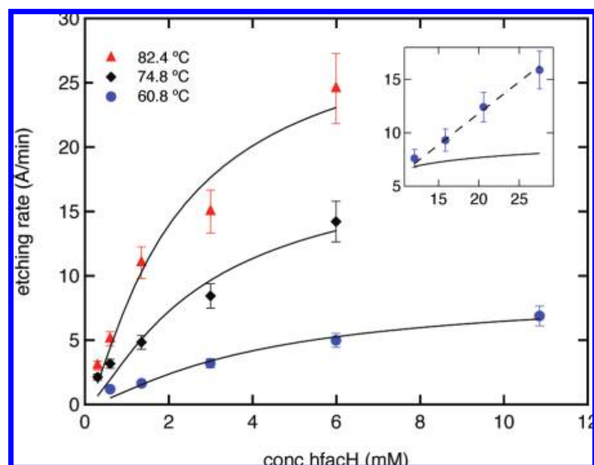

Figure 9. Comparison of experimental CuO etching data to the proposed model given in eq 6 at 60.8, 74.8, and 82.4 °C. The error bars correspond to the propagated error from uncertainties in the CuO film thickness and etching time. The inset shows the reaction model extrapolated to hfacH concentrations above 11 mM at 60.8 °C, with the dashed line representing a linear model.

diffusion coefficient of hfacH in $scCO_2$ is reported to be on the order of 10^{-4} cm^2/s,[45] predicting a Da_s value of 10^{-3}. The diffusion coefficient is so high that there was no significant diffusion resistance in the fluid, and the surface reaction governs the etching rate. This was expected since the hfacH concentration chosen for rate measurements was relatively low and supercritical fluids typically provide high mass transport.

The primary reaction rate parameters K_A and k_2 were extracted through nonlinear fitting of the experimental rate data to eq 6 using the Levenberg–Marquardt method. A first approximation of the values was obtained from a least-squares fit of the linearized equation developed under the limiting condition of infinite K_D. Due to the discontinuity in reaction order at high hfacH concentrations, the reaction rate parameters were generated using only the low hfacH concentration regime (0.3–10.9 mM). Table 1 shows the best fit values for K_A (mM^{-1}) and k_2 (Å/min) at each of the temperatures studied. The equilibrium constant for step 3, K_D, could not be directly obtained because experimental data showed no correlation between excess $Cu(hfac)_2 \cdot H_2O$ in solution and the reaction rate (Figure 7). However, sensitivity analysis revealed that by assuming fast desorption and setting $K_D \geq (3.0 \times 10^2)K_A$, the $Cu(hfac)_2 \cdot H_2O$ concentration could be varied up to 9.0 mM with less than 10% variation in the modeled etching rate. Error between the experimental data and eq 6 was minimized as k_{-2} approached 0. This suggests that, under the conditions studied, step 2 is nearly irreversible. The Langmuir–Hinshelwood model with the fit parameters K_A and k_2 in Table 1 closely represented the data from 60.8 to 82.4 °C below an 11 mM hfacH concentration as shown in Figure 9; at this concentration and 60.8 °C, this model predicts that the fractional hfac surface coverage is 0.85.

A single model could not be used to fit both the low and high concentration regimes of the rate data gathered at 60.8 °C. Below 11 mM, the data exhibited a reaction order of approximately 0.6 and were accurately represented by the Langmuir–Hinshelwood rate expression given in eq 6. At higher concentrations, the rate approached an order of 1, suggesting a shift in the dominant etching mechanism. As the hfacH concentration increased, the available CuO surface sites decreased to a fractional coverage of 0.15, which could be the point where initial adsorption of hfacH in step 1 becomes rate limiting. In this case, the reaction order would exhibit a first-order dependence. Moreover, as a CuO surface is covered by hfac ligands, the probability of an hfacH from the fluid phase striking a filled site increases; this Rideal–Eley mechanism also predicts a first-order dependence of the rate on the hfacH concentration (see the Supporting Information). The high concentration regime of the 60.8 °C data is plotted in the inset of Figure 9. The solid line represents the extrapolated eq 6 Langmuir–Hinshelwood rate expression, and the dashed line shows an improved fit from a linear adsorption-limited or Rideal–Eley model. A similar transition in the etching mechanism should occur at higher temperatures, but the time to remove the film was too short to measure accurately above an hfacH concentration of ~8 mM.

Model fits of the rate data predicted that K_A is proportional to the temperature (Table 1). Chemisorption processes are typically exothermic and exhibit adsorption equilibria with an inverse relationship to temperature; however, etching in $scCO_2$ at constant pressure and increasing temperature from 60.8 to 82.4 °C decreased the solvent density from approximately 0.66 to 0.51 g/cm^3, which can also affect the adsorption behavior. The solubility parameter for hfacH, δ_{hfacH}, was calculated from Δh^{vap}_{hfacH} [28] and is approximately 14.0 (J cm^{-3})$^{1/2}$. Comparatively, δ_{scCO_2} is a function of the density and decreased from 11.5 to 8.9 (J cm^{-3})$^{1/2}$ between 60.8 and 82.4 °C.[39] At higher reaction temperatures, the difference between δ_{hfacH} and δ_{scCO_2} was greater, so hfacH became less soluble in $scCO_2$. The reduced solubility caused hfacH molecules to favor surface coordination over fluid interactions, shifting the equilibrium toward adsorption and effectively increasing K_A. This phenomenon has been reported for other systems, including processes with organometallic species. One example is bis(2,2,6,6-tetramethyl-3,5-heptanedionato)(1,5-cyclooctadiene)ruthenium(II) adsorption on carbon aerogels in $scCO_2$.[46] Maintaining constant pressure while increasing the temperature by 20 °C resulted in a proportional adsorption uptake on the aerogel particles. For CuO removal, the temperature dependence of K_A includes counteracting effects from the changing solution density ($T\uparrow$, $K_A\uparrow$) and the ΔH_{ads} of hfacH ($T\uparrow$, $K_A\downarrow$), with the density effect dominating to produce an observed increase in K_A with increasing temperature. Accounting for adsorption changes with the solution density is a feature of the reaction model that accurately represents the CuO etching process.

The overall temperature dependence of the CuO etching rate also relies on the rate coefficient for step 2, k_2. Arrhenius analysis of k_2 between 60.8 and 82.4 °C yielded an activation energy of 55.6 ± 4.0 kJ/mol. This is lower than the 81 kJ/mol activation energy reported for the proposed disproportionation reaction of two Cu–hfac moieties in gas-phase CuO etching between 170 and 240 °C.[31] Reactive pathways for etching CuO

(45) Yang, X.; Matthews, M. A. *J. Chem. Eng. Data* **2001**, *46*, 588.

(46) Zhang, Y.; Cangul, B.; Garrabos, Y.; Erkey, C. *J. Supercrit. Fluids* **2008**, *44*, 71.

with hfacH in the gas phase and in $scCO_2$ are likely similar, but favorable solvent interactions enable analogous reactions to proceed at lower temperatures in $scCO_2$. These solvation forces could act to stabilize intermediate species, thus reducing the activation barrier and facilitating low-temperature etching. Further evaluation of the model rate expression in eq 6 can be made by comparison with the experimental rate behavior as a function of temperature (Figure 5). The model is a function of both K_A and k_2, but exhibits a higher sensitivity toward k_2. Substituting both temperature-dependent parameters back into the reaction model predicts an apparent activation energy of 76.6 ± 1.2 kJ/mol over the temperature range 53.5−88.4 °C, which is close to the measured value of 70.2 ± 4.1 kJ/mol.

Water Effects. In this study, it was found that adding up to 10× the molar ratio of water to hfacH on the basis of eq 1 nearly doubled the nominal CuO etching rate (5× the concentration of hfacH on a direct molar basis). While this experimental trend contradicts Le Chatelier's principle, there have been other reports of water promoting reactions between β-diketones and metal species. For example, the addition of small amounts of water increased scandium metal solubility in neat liquid hfacH as well as various other metals in several β-diketones.[47] A similar effect was reported in the extraction of both stainless steel[4] and trivalent lanthanide ions[48] with β-diketones and water in $scCO_2$. In the case of stainless steel, the catalytic effect leveled off at a water concentration of approximately 2.7 times the molar amount of hfacH.[4] Interestingly, low concentrations of water have also proven beneficial for Cu deposition from metal chelate complexes.[49] Water increased gas-phase Cu deposition from hfac(Cu)L, where L is a neutral ligand, by accelerating dissociation of the metal complex through hydrogen bonding with an attached hfac ligand.[49] Collectively, these literature results substantiate the observation of water increasing reactivity during metal chelation, though the exact mechanism for enhancement might vary depending on the specific reaction process.

During $scCO_2$ etching, water could have increased the reaction rate by interacting with either the CuO surface or hfacH in solution. Reaction of CuO with water can form $Cu(OH)_2$, which has been reported to etch more quickly than CuO.[10] However, XPS analysis showed that exposing Cu metal and CuO films to 10× H_2O in $scCO_2$ did not change the state of Cu, indicating water did not affect the sample surface at the concentrations studied. Additionally, excess water reacting directly with the CuO surface would have competed for surface sites and caused the reaction rate to decrease at high concentrations, rather than the observed saturation behavior (Figure 8). Hence, it is more probable that water enhanced the rate by interaction with fluid-phase hfacH molecules, possibly forming an activated chelating species. Note that excess $Cu(hfac)_2 \cdot H_2O$ did not affect the reaction rate (Figure 7), implying water must be uncoordinated to react.

In contact with pure water, hfacH hydrolyzes to form either the *gem*-diol $hfac(OH)_4$ or the enolate ion $hfac^-$ shown in Scheme 2.[50−52] Decomposition products such as CF_3COO^- and CF_3COCH_3 may also form, but only after extended reaction times.[52] No equilibrium species data are currently published on the three-component system of hfacH and water in $scCO_2$. Although the *gem*-diol form prevails in the two-phase hfacH−H_2O system, large, hydrated molecules are typically not stable in CO_2, and a lack of nucleophilic O atoms would prevent interaction with CuO. The most likely speciation in CO_2 involves formation of a complex where a water molecule hydrogen bonds to the acidic hfacH proton and partially dissociates it (Scheme 2). Full dissociation of the proton is unlikely because formation of the enolate and hydronium ion pair is unfavorable in nonpolar $scCO_2$. Studies on the interaction of organic acids with polar entrainers in $scCO_2$ have shown that H-bonds between the acid and polar cosolvent can form, resulting in increased polarity and nucleophilic activity of the bonded molecule.[53−55]

Scheme 2. Reaction between hfacH and H_2O[a]

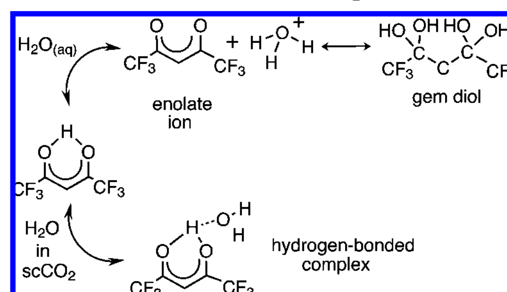

[a] In aqueous solution, water and hfacH form the enolate/hydronium ion pair and the *gem*-diol. In $scCO_2$, water and hfacH form a hydrogen-bonded complex.

Formation of an activated hfacH species provides an explanation for the increased reactivity of hfacH and water with CuO. The strong nucleophilic character of a H-bonded complex would accelerate attack of ∼O−Cu−O∼ and shift the step 1 equilibrium further toward adsorption. Increasing the water concentration in solution drives the generation of activated hfacH and enhances the rate by increasing K_A. Analysis of eq 6 shows that even subtle changes in K_A will impact the etching rate. The observed 2-fold increase in the etching rate in the presence of excess water can be predicted by increasing K_A from its modeled value of 0.75 to 1.6 mM^{-1} at 74.8 °C. Although the ionic character of a hydrogen-bonded hfacH species would render it less stable in CO_2, nonreacting water in solution could have aided solubility. Inclusion of polar entrainers is known to improve $scCO_2$ solubility of polar molecules through a variety of complex factors including increased solution polarizability and density.[56]

There are at least two scenarios that could have caused the catalytic effect of water to plateau at approximately 10× the concentration of hfacH. It is possible that the amount of hydrogen-bonded hfacH saturated the CuO surface with ∼O−Cu−hfac, thus negating any further increase in concentration of the activated reactant. The fraction of open CuO sites is a function of the hfacH concentration and, without water, had an equilibrium value of approximately 0.5. As more hydrogen-bonded hfacH was produced, the coverage of ∼O−Cu−hfac

(47) Sievers, R. E.; Connolly, J. W.; Ross, W. D. *J. Gas Chromatogr.* **1967**, *5*, 241.
(48) Lin, Y.; Wai, C. M. *Anal. Chem.* **1994**, *66*, 1971.
(49) Jain, A.; Kodas, T. T.; Corbitt, T. S.; Hampden-Smith, M. J. *Chem. Mater.* **1996**, *8*, 1119.
(50) Aygen, S.; van Eldik, R. *Chem. Ber.* **1989**, *122*, 315.
(51) Ellinger, M.; Duschner, H.; Stark, K. *J. Inorg. Nucl. Chem.* **1978**, *40*, 1063.
(52) Duschner, H.; Stark, K. *J. Inorg. Nucl. Chem.* **1978**, *40*, 1387.
(53) Ke, J.; Jin, S.; Han, B.; Yan, H.; Shen, D. *J. Supercrit. Fluids* **1997**, *11*, 53.
(54) Iwai, Y.; Tanabe, D.; Yamamoto, M.; Nakajima, T.; Uno, M.; Arai, Y. *Fluid Phase Equilib.* **2002**, *193*, 203.
(55) Renault, B.; Cloutet, E.; Cramail, H.; Tassaing, T.; Besnard, M. *J. Phys. Chem. A* **2007**, *111*, 4181.
(56) Dobbs, J. M.; Wong, J. M.; Lahiere, R. J.; Johnston, K. P. *Ind. Eng. Chem. Res.* **1987**, *26*, 56.

would have increased and possibly reached a rate-limiting value. A second explanation is convergence to the solubility limit of activated hfacH in $scCO_2$. The polar nature of hydrogen-bonded hfacH would have rendered it less soluble than either hfacH or water alone. Once it reached maximum solubility, equilibrium of the H-bonded complex would shift back into an uncoordinated form, and no further impact on the rate would be observed.

Conclusions

The kinetics for etching thin CuO films with the metal chelator hfacH in $scCO_2$ were studied and used to develop a reaction mechanism. Analysis of the surface reaction in the context of the rate behavior revealed details of the mechanism relevant to advancing heterogeneous reactions in $scCO_2$, specifically nanoscale metal synthesis. In contrast to the analogous gas-phase reaction where temperatures greater than 150 °C are required for etching,[31,32,35] copper removal was observed at temperatures as low as 53.5 °C. Supercritical fluid processing is known to enhance certain reactions[11] and, in this case, was a result of CO_2 solvation forces reducing the activation energy of the rate-determining step. This behavior could be exploited for processing heat-sensitive materials including metal–organic composites. Below an hfacH concentration of 11 mM, the apparent reaction order was ~0.6, and CuO etching was modeled with a three-step Langmuir–Hinshelwood scheme consisting of (1) dissociative adsorption of hfacH on a CuO site, (2) surface reaction between two adsorbed hfacH molecules to generate $Cu(hfac)_2$ and water, and (3) desorption of the product species. Above an hfacH concentration of 11 mM, the apparent reaction order was ~1 due to adsorption-limited etching or to the increased probability of an hfacH molecule in the fluid striking a filled surface site. Understanding the mechanism change as a function of the reactant concentration could be utilized to tune surface structures. Just like changes in temperature and pressure alter the density of $scCO_2$, which can affect a reaction rate, increasing the concentration of a molecule dissolved in $scCO_2$ can cause a switch from a mechanism that is gaslike to one that is liquidlike. Although etching rates in this study were intentionally kept low for detailed kinetic analysis, the experimental data can be extrapolated to predict a rate greater than 10 nm/min at hfacH concentrations of approximately 100 mM and a moderate temperature of 74.8 °C. This rate could be increased further by addition of catalytic amounts of water, which was shown to enhance the reaction through the proposed formation of a hydrogen-bonded hfacH species.

Acknowledgment. Funding for this project was provided by Texas Instruments through a Semiconductor Research Corp. (SRC) customized research grant. We are grateful to Gerardo Montano for assistance with computer programming and Gary Chandler (Department of Material Science, University of Arizona) for SEM images. R.M. gratefully acknowledges support from the AAUW Selected Professions Fellowship, the ARCS Foundation, and the University of Arizona Chapman Fellowship Program.

Supporting Information Available: Process flows, full scan XPS spectra, and a kinetic model for a Rideal–Eley mechanism. This material is available free of charge via the Internet at http://pubs.acs.org.

JA8050662